A Template and Catalyst-Free Metal-Etching-Oxidation Method to Synthesize Aligned Oxide Nanowire Arrays: NiO as an Example

Zhi Peng Wei,[†] Miryam Arredondo,[‡] Hai Yang Peng,[†] Zhou Zhang,[†] Dong Lai Guo,[†] Guo Zhong Xing,[†] Yong Feng Li,[†] Lai Mun Wong,[§] Shi Jie Wang,[§] Nagarajan Valanoor,[‡] and Tom Wu*,[†]

[†]Division of Physics and Applied Physics, School of Physical and Mathematical Sciences, Nanyang Technological University, Singapore 637371, [‡]School of Materials Science, University of New South Wales, Sydney NSW 2052, Australia, and [§]Materials Science and Characterization Cluster, Institute of Materials Research and Engineering, Singapore 11760

ABSTRACT Although NiO is one of the canonical functional binary oxides, there has been no report so far on the effective fabrication of aligned single crystalline NiO nanowire arrays. Here we report a novel vapor-based metal-etching-oxidation method to synthesize high-quality NiO nanowire arrays with good vertical alignment and morphology control. In this method, Ni foils are used as both the substrates and the nickel source; $NiCl_2$ powder serves as the additional Ni source and provides Cl_2 to initiate mild etching. No template is deliberately employed; instead a nanograined NiO scale formed on the NiO foil guides the vapor infiltration and assists the self-assembled growth of NiO nanowires *via* a novel process comprising simultaneous Cl_2 etching and gentle oxidation. Furthermore, using CoO nanowires and Co-doped NiO as examples, we show that this general method can be employed to produce nanowires of other oxides as well as the doped counterparts.

KEYWORDS: nickel oxide · nanowire · metal-etching-oxidation method · catalyst · self-assembly

Deterministic synthesis of one-dimensional (1D) crystalline nanowires (NWs) with controlled morphologies and properties is currently a major objective in nanosciences and nanotechnologies.[1] Various synthesis routes have been developed, and their applications to NW synthesis have been intensively pursued. Compared with the solution-based methods, vapor transport growth has the advantage of being more environmentally friendly and often can give NWs with high aspect ratios, which is critical for many key applications. Vapor−liquid−solid (VLS) growth is one of the most popular synthesis methods, where liquid-state catalyst nanoparticles absorb the precursor vapor and NW growth starts when supersaturation is reached in the nanoparticles.[2−5] Recently, a variant that uses solid-state catalysts at lower temperatures, termed as the "vapor−solid−solid" (VSS) growth, has also been devised to grow NWs.[6] In another distinct approach without the use of catalyst, NW synthesis has been accomplished through the vapor−solid (VS) route.[7,8] Among all the techniques to produce NWs, the hot plate method is probably the most convenient and cost-effective, where heating metal foils in either atmosphere or controlled environment was found to give 1D nanomaterials.[9] Complementary to the above vapor-based routes, template-assisted methods have been employed to produce NWs with uniform size; for example, liquid or gas phase precursors were filled into the pores of anodic aluminum oxide (AAO) membranes to render either NWs or nanotubes.[10]

However, it is well recognized that for some materials the currently available synthesis methods are not very effective to enable the anisotropic growth of 1D NWs. This is in particular true for materials with cubic crystal symmetries which lack the structural anisotropy critically needed for the growth of single crystalline NWs. Synthesis of these oxide NWs requires developing novel routes beyond the conventional ones. Nickel oxide (NiO) is one of such notable materials. NiO is an important member in the family of binary oxides with a cubic rock salt structure and a lattice parameter of 0.4195 nm. Several decades ago, NiO played a very critical role in the development of the modern solid state physics by revealing the limitation of the free electron model and the critical role of strong electron correlation.[11] Today, NiO is an important p-type semiconductor

*Address correspondence to tomwu@ntu.edu.sg.

Received for review March 16, 2010 and accepted July 01, 2010.

Published online July 8, 2010.
10.1021/nn1005396

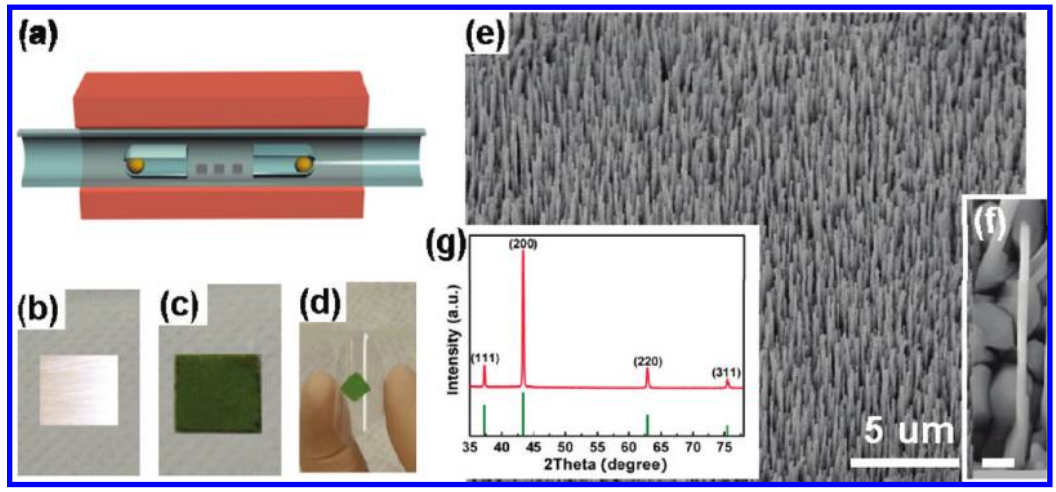

Figure 1. (a) Schematic of the experimental setup. This figure is not drawn to scale. Photographs of (b) polished Ni foil, (c) Ni foil after NiO NW growth, and (d) NiO NW arrays after being transferred from the Ni foil to a flexible plastic substrate. (e) A typical SEM image of the NiO NW arrays. (f) SEM image of an individual NiO NW. The scale bar is 200 nm. (g) XRD spectrum of the NiO NW arrays. The NiO powder diffraction data (JCPDS Card No. 78-0423) is also shown at the bottom.

material[12] and has been extensively investigated because of its myriad applications in catalysts,[13,14] gas sensors,[15] battery materials,[16] electrochromic coatings,[17] and so on. It is also a canonical antiferromagnetic material with a Neel temperature of 523 K,[18] and often used in magnetic multilayer devices.[19,20] Most recently, NiO showed excellent resistive switching behaviors and may find potential uses in nonvolatile memories.[21,22] Up to now, a variety of methods have been attempted to achieve nanostructured NiO, but all of them suffer from drawbacks. For example, solution-based chemical routes[23] and sol−gel methods[24] were shown to produce NiO NWs in large quantity, but the NWs have no alignment. Electrochemical deposition into anodic alumina membranes[25,26] and oxidation of NiS precursor in molten salt[27] were also employed to prepare NiO NWs. However, these two methods lead to only polycrystalline NWs. To the best of our knowledge, template-free synthesis of aligned single-crystal NiO NW arrays has not been reported.

In this study, we discovered a novel template- and catalyst-free method to synthesize high quality NiO NW arrays. This facile method involves controlled anisotropic etching of a nickel (Ni) foil through a NiO layer with low-pressure Cl_2 vapor, which is accompanied by continuous oxidation. It is the first time, to our knowledge, that single-crystal NiO NW arrays were synthesized with a template-free method. Furthermore, we show that this method is a general approach to produce metal oxide NW arrays and can be used to dope the NWs by adjusting the vapor source.

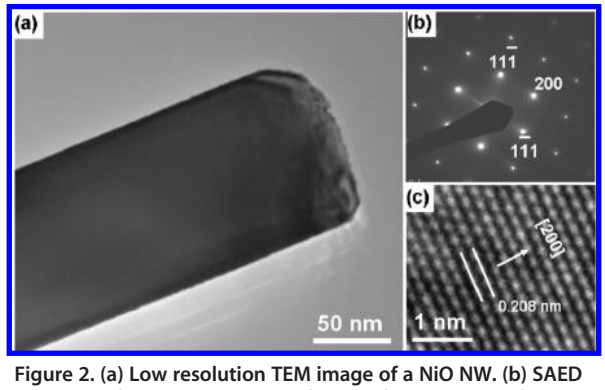

Figure 2. (a) Low resolution TEM image of a NiO NW. (b) SAED pattern and (c) HRTEM image taken on the same NW. The interplane distance of 0.208 nm is consistent with the lattice constant of NiO.

RESULTS AND DISCUSSION

The synthesis of the NiO NW arrays was carried out in a home-built vapor transport system comprising a horizontal tube furnace (Lindberg/Blue mini-mite) and a gas delivery and pumping system as described previously.[28−30] The schematic of the experimental setup is shown in Figure 1a. Ni foils were cut into small pieces, cleaned, mechanically polished, and electrochemically polished. Finally, the Ni foils were annealed to decrease the internal stress and to further improve the crystalline quality (see Supporting Information Figure S1). These presynthesis treatments are critical to achieve (100) textured Ni foils with very flat surfaces. The treated Ni foils (Figure 1b) were then put in the center of the furnace between the small tubes containing the $NiCl_2$ powder. We need to point out here that the Ni foils serve as both the substrate and the nickel source. Nickel chloride ($NiCl_2$) powder was put into two small one-end-open quartz tubes. After the growth process, a layer of green products was grown on the surface of the Ni foils. Figure 1c shows the optical image of the Ni foil after growth. The green color indicates the presence of NiO on the Ni foil. We found that NiO NWs are not directly grown on the Ni foil, but imbedded under a NiO film (the growth mechanism will be discussed in details later on). Thus to reveal the NiO NW arrays, we need to bond a supporting substrate to the sample using either silver paste or double-sided tape, then the NiO NWs can be conveniently transferred to the sub-

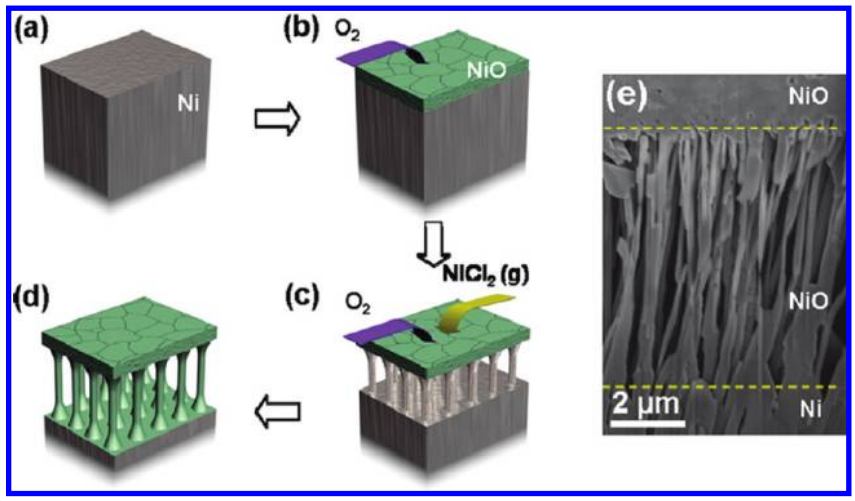

Figure 3. Schematic of the metal-etching-oxidation (MEO) mechanism proposed for the growth of NiO NW arrays. (e) Cross-sectional SEM image of the NiO NW arrays prepared by focused ion beam (FIB) milling.

strate by lift-off. Since the growth and transfer processes are separated, a supplementary advantage of this method is that there is no limitation on selecting the final supporting substrate. Figure 1d shows the optical image of a sample of NiO NW arrays being transferred to a flexible plastic substrate. Figure 1e shows a typical SEM image of the NiO NW arrays. The NiO NWs are several micrometers in length and about one hundred nanometers in diameter. They are quite uniform and appear well aligned. Figure 1f is the SEM image of an individual NiO NW showing a smooth surface. The chemical composition of the NWs was characterized by XRD, and as shown in Figure 1g, only NiO related peaks were detected. The relative intensity of the peaks differs from the powder diffraction data (JCPDS Card No. 78-0423), and the dominant (200) peak indicates a preferred (200) orientation. The absence of $NiCl_2$ or Ni related peaks excludes the existence of any impurity phase above the detection level.

The crystalline structure of the NiO NWs was further characterized by TEM. Figure 2a shows a low-resolution TEM image of a NiO NW. The diameter of this particular NW is about 130 nm. The selected area electron diffraction (SAED) pattern in Figure 2b can be indexed as the cubic structure with no detectable secondary phase. The HRTEM image (Figure 2c) was recorded along the [011] zone axis and it shows clear lattice fringes. The distance between the lattice planes along the NW growth direction is 0.208 nm, which is consistent with the lattice constant of the NiO unit cell. Both the SAED pattern and the HRTEM image suggest that the NW is single crystalline and the growth direction is along [200]. Among a dozen NiO NWs we examined using HRTEM, we also observed a few growing along [220] (Supporting Information, Figure S2). Nevertheless, we found that the majority of the NiO NWs are along the [200] direction, which is in agreement with the XRD data.

We now discuss the tentative formation mechanism of the NWs which grow underneath the NiO overlayer. The schematic in Figure 3a−d illustrates the growth process of the NiO NW arrays. At the growth temperature, three major reactions are involved:[31]

$$Ni(s) + 1/2O_2(g) \rightarrow NiO(s) \quad (1)$$

$$NiCl_2(g) + 1/2O_2(g) \rightarrow NiO(s) + Cl_2(g) \quad (2)$$

$$Ni(s) + Cl_2(g) \rightarrow NiCl_2(g) \quad (3)$$

The high temperature oxidation of Ni and the formation of NiO scale have been studied for many years.[32] The oxidation reaction in eq 1 accelerates as the furnace temperature increases, which is accompanied by a weight gain of the Ni foil (Supporting Information, Figure S3). The formation of NiO is also confirmed by the XRD data shown in Figure S4; the NiO [200] peak at 43.3° starts to appear and becomes stronger as the temperature increases. When the furnace temperature reaches 600 °C, $NiCl_2$ powder starts to evaporate into the gas form, which is evidenced by the rapid weight loss of the $NiCl_2$ powder above this temperature (Figure S3). The reaction 2 suggests that $NiCl_2$ vapor reacts with O_2 in the mixture gas to produce Cl_2 gas. The existence of Cl_2 gas can significantly affect the kinetics of the oxidation process.[31] It is important to note that there are many closely spaced microchannels across the columnar NiO scale, and the gaseous species can penetrate the scale along the fine grain boundaries.[32] Subsequently, according to reaction 3, the Cl_2 gas diffuses through the NiO layer and etches the Ni substrate underneath it. This process helps to gently sculpt the continuous Ni foil into wire-like morphology as illustrated in Figure 3c. According to the reaction 3, during etching, additional $NiCl_2$ is produced in the gas form, which is fed back to reaction 2. Hence, $NiCl_2$ and Cl_2 are conserved, and the overall result is the oxidation of Ni. However, this balance is not strictly maintained in the experiments; $NiCl_2$ and Cl_2 in the gas form continuously

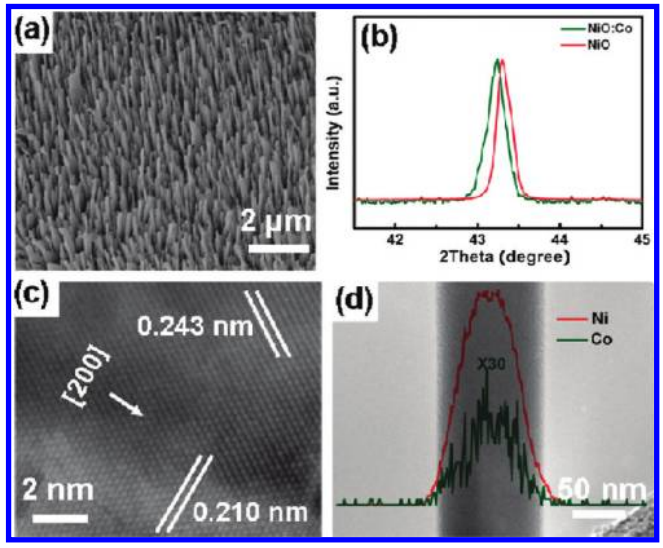

Figure 4. (a) SEM image of Co-doped NiO NW arrays obtained by using $CoCl_2$ as the source powder. (b) The normalized (200) peak in XRD pattern of the NiO and Co-doped NiO NW arrays. (c) HRTEM image showing the growth direction along [200]. (d) EDS mappings of Ni and Co across an individual NW.

escape from the samples and flow away with the carrying gas, which eventually terminates the reactions.

We should note that although no template is deliberately employed in the synthesis, the nanograined NiO scale serves as a mask guiding the infiltration of Cl_2 and O_2 gases. As illustrated in the schematics in Figure 3, concurrent to the etching process is the oxidation of Ni into the NiO NWs, which is sustained by the carrying gas. During this process, the electric field of more than 10^6 V cm^{-1} developed between Ni and NiO,[33] along with the giant mechanical stress at the interface,[34] may assist the self-organized formation of the NiO NW arrays. It has been reported that in the oxidation of highly textured Ni tapes the crystallographic orientation of the NiO grains is closely correlated with that of the Ni grains underneath.[35] Therefore, the annealing process prior to the NW growth helps to produce highly textured Ni foils and warrants the crystalline alignment of the produced NiO NW arrays. Furthermore, the NiO scale with fine channels limits the reaction rate and helps to protect the Ni foil from being etched excessively. If the oxidation proceeds too fast, the growth stress may cause the oxide to separate from the metal due to the insufficient oxide plasticity.[36] This is analogous to the recently reported spontaneous growth of $NiSi_x$ NWs where polygrained NiO_x overlayers act as a diffusion barrier to kinetically and spatially control the Ni diffusion during the chemical vapor growth.[37,38] It was shown that the presence of the oxide overlayers on Ni seed layers promote the reproducible one-dimensional growth of $NiSi_x$ single crystals. Similarly, oxide overlayers play critical roles in our experiments to control the vapor supersaturation and to give the reliable NiO NW growth.

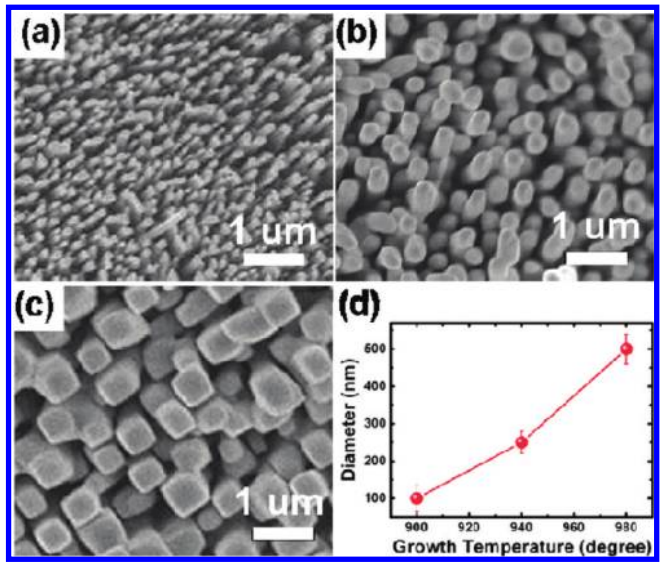

Figure 5. Effect of the growth temperature on the morphology of NiO NW arrays. Typical SEM images taken on samples grown at substrate temperatures of (a) 900, (b) 940, and (c) 980 °C. (d) Dependence of the NW diameter on the growth temperature.

We suggest to term this approach of producing aligned NiO NW arrays the "metal-etching-oxidation" (MEO) process which captures the essence of the formation mechanism. Furthermore, to achieve direct evidence to confirm the above scenario, we looked at the cross-sectional SEM image of the NW arrays exposed by using focused ion beam (FIB) milling. As shown in Figure 3e, the NiO NWs are imbedded between the NiO scale layer and the Ni foil. Even though significant breaking, melting, and fusing of the NiO NWs occurred because of the large ion milling current, the observed particular columnar structure of the NiO NW arrays supports the proposed growth mechanism. However, we should be cautious regarding to the details of the exact growth mechanism owing to the lack of direct experimental evidence and real-time observation. We noted that anisotropic silicon NW arrays have been recently fabricated *via* a metal-assisted chemical etching method.[39,40] Although both the reported method and ours rely on anisotropic etching, our approach does not involve the use of any catalyst and appears to be more suitable to prepare NWs of metal oxides.

Since etching and oxidation are the two key elements in the MEO process, chlorides other than $NiCl_2$ should also be capable to initiate the growth. To test this hypothesis, we chose $CoCl_2$ as the source powder in the synthesis. At high temperatures, Cl_2 gas is produced as the following:

$$CoCl_2(g) + 1/2O_2(g) \rightarrow CoO(s) + Cl_2(g) \qquad (4)$$

Following a similar growth mechanism as in the $NiCl_2$ case, NW arrays were obtained. As shown in Figure 4a, the NW arrays are uniform, being 2 μm in length and about 100 nm in diameter. In addition, this change of source allows us to introduce Co as a doping element into the NiO NWs. The Co doping process occurs simul-

taneously with the etching and oxidation process, and the high synthesis temperature assists the efficient diffusion of Co in the NiO matrix. As shown in the XRD patterns in Figure 4b, the (200) peak of the Co-doped NiO NWs shifts toward a lower angle compared with that of the undoped counterpart, which is consistent with the fact that the radius of Co ions (0.0838 nm) is slightly larger than that of the Ni ions (0.0830 nm). The HRTEM image in Figure 4c shows that the single crystal NWs grow along the [200] direction, consistent with the results of the NiO NWs. The EDS data suggest a Co doping level of *ca.* 1%. In addition, in the EDS line scans across an individual Co-doped NiO NW (Figure 4d), the Co profile appears to follow the Ni profile very well, indicating a uniform distribution of the Co element.[41]

We further demonstrate that one is able to tune the morphology of the NiO NWs through adjusting the growth temperature and the oxygen content in the carrying gas. As shown in the SEM images in Figure 5a−c, the diameter of the NiO NWs increased from 100 to 500 nm as the growth temperature changed from 900 to 980 °C. This clear trend shown in Figure 5d could be due to two reasons. One is that a higher growth temperature always results into a NiO scale with larger grains.[42] Since the NW morphology is mainly defined by the Cl_2 gas etching through the grain boundaries, larger grains eventually lead to thicker wires. The other is that a higher temperature significantly promotes the Ni oxidation, thus circumvents the etching, which may also result in NWs with larger diameters. At 980 °C, the cross section of the NiO NWs appears to be square-like, indicating their single crystal nature.

We found that the growth temperature has little effect on the length of the NiO NWs. Instead, the NW length can be well controlled by adjusting the gas content. As shown in the SEM images in Figure 6a−d, shorter NWs could be obtained if a carrying gas with lower oxygen content was used. The length and diameter of NWs were measured for these samples, and the statistical results are shown in Figure 6e and f. The NW length increased from 1 to 10 μm with the increasing oxygen content from 0.5% to 15%, while the diameter changed only slightly. This effective length control originates from the fact that a higher oxygen concentration promotes the oxidation and protects the NW core from the excessive etching. Consequently, the Cl_2 etching gas goes deeper into the Ni foil, forming longer NiO NWs. Since the diameter and the length of the NiO NWs can be independently controlled by the growth temperature and the carrying gas content, the synthesis route herein gives lots of flexibility in the morphology control.

Recently NiO thin films have been reported for their potential applications in the next generation resistive RAM (ReRAM) devices, which may serve as alternatives to the current nonvolatile flash memory technology.[43,44] Although the switching model involving the formation and rupture of conducting filaments is widely used to explain the experimental observations, the complex switching mechanisms in NiO warrants further investigations. Very recently, reversible resistive switching behaviors have been demonstrated in NiO nanowires fabricated in anodized aluminum oxide membranes[13] and MgO/NiO core/shell heterostructured NWs.[45] Our preliminary results suggest that the NiO NW arrays grown by the MEO method also show bipolar resistive switching (Figure 7). We scratched near the edge of the sample to reach the Ni foil underneath the NWs, and then the exposed Ni foil and a Pt pad deposited on the NiO NW arrays served as the electrodes for the switching experiments (the inset of Figure 7). When a voltage was applied as 0 → 4 V, the current through the Pt/NiO/Ni device increased dramatically

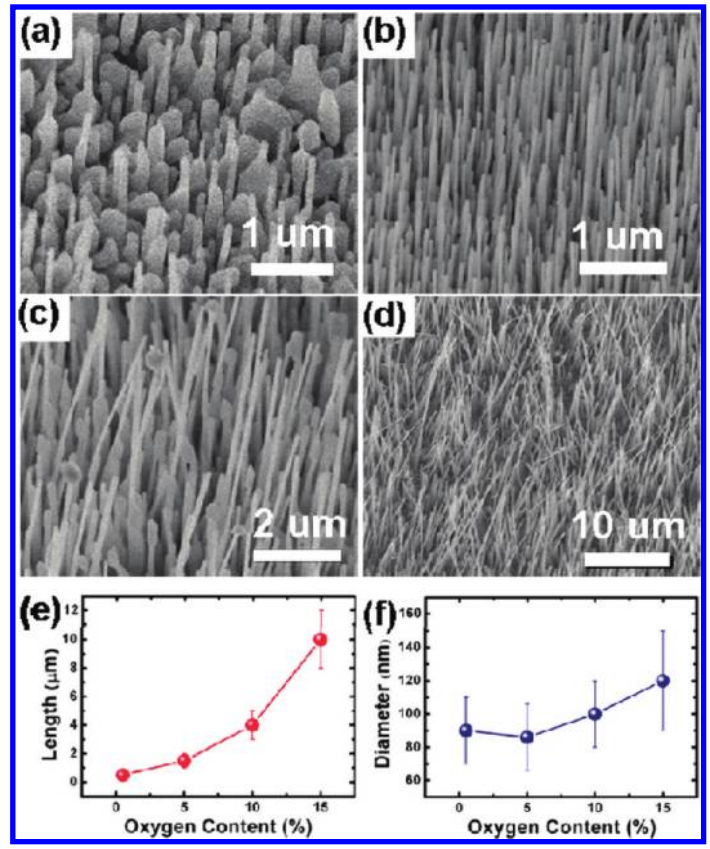

Figure 6. Morphology evolution of the NiO NW arrays with different growth atmospheres: (a) 0.5% O_2, (b) 5% O_2, (c) 10% O_2, and (d) 15% O_2 in the carrying gas. (e) Dependence of the NW length on the oxygen content. (f) Dependence of the NW diameter on the oxygen content.

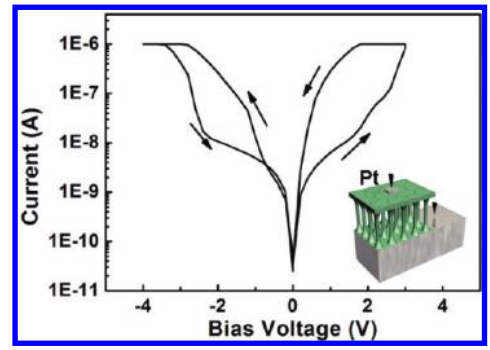

Figure 7. *I*−*V* characteristics of the NiO NW arrays. Inset shows the schematic diagram of the measurement.

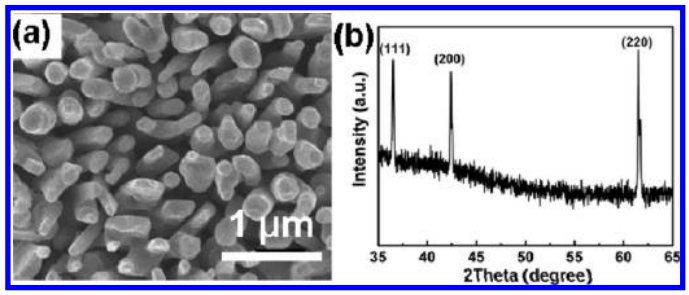

Figure 8. Top-view SEM image and XRD data of cobalt oxide (CoO) NW arrays.

to the μA range, indicating a "SET" process. The device can be switched back to the initial high resistance state by applying a voltage sweep as 0 → −4 V, indicating a "RESET" process. The ON/OFF ratio between the high resistance state and the low resistance state reached 2 orders of magnitude.

Furthermore, the novel synthesis approach presented here can also be applied to other metal oxides. One prerequisite of the application of this method is the formation of a thin granular oxide scale covering the metal foil which critically facilitates the etching process. Considering that the Gibbs energy of forming CoO is similar to that of forming NiO,[46] we tried our MEO method on the fabrication of CoO NW arrays. Indeed we found that CoO NW arrays can also be grown on Co foils following a similar route, as shown in Figure 8a. Our preliminary results suggest that, similar to NiO, NWs of CoO can also be grown *via* the MEO method. In this case, we used Co foils as the substrate and $CoCl_2$ as the source. The experimental growth conditions are similar to those for the growth of NiO NWs. As shown in the SEM picture, the CoO NW quality is yet to be optimized; the NWs appear shorter than the NiO counterpart and the NWs diameters are not uniform. Nevertheless, the XRD data in Figure 8b suggests that the growth product is CoO without second phase. Thus these preliminary results encourage the application of this MEO method to the synthesis of other metal oxide nanowires.

CONCLUSIONS

Single crystal NiO NW arrays have been synthesized for the first time through a facile vapor-based metal-etching-oxidation method. The diameter and the length of the nanowire can be well controlled by adjusting the growth temperature and the carrying gas content. Furthermore, by replacing $NiCl_2$ with $CoCl_2$ in the source powder, uniform Co doping can be introduced in the NiO NWs. We also used CoO as an example to demonstrate that this method can be applied to synthesize NWs of other oxides. In the general context, it is well-known that materials belonging to the high-symmetry cubic space groups are notoriously difficult to grow into anisotropic single crystalline nanowires. Therefore, our method presents a novel and general route to synthesize low dimensional metal oxide nanostructures, and will help to advance the research on their functionalities and applications.

EXPERIMENTAL SECTION

Nanowire Synthesis. The synthesis of the NiO NW arrays was carried out in a home-built vapor transport system comprising a horizontal tube furnace (Lindberg/Blue mini-mite) and a gas delivery and pumping system.[28−30] $NiCl_2$ power with a weight of 0.1 g (Aldrich, 98%) was introduced into two one-end-open quartz tubes and put opposite to each other in the middle of the furnace quartz tube. Ni foils (0.125 mm thick, Aldrich 99.9%) were cut into small pieces with a typical size of 10 mm × 10 mm and cleaned by acetone. After cleaning, the foils were mechanically polished using a Buehler MiniMet 1000 polisher, following three step: (1) polishing with SiC paper disks (120-grit) under water cooling; (2) using rigid grinding disks (Metadi Supreme, 3-μm PC); (3) using microcloth pad with 0.05-μm alumina suspension. Subsequently, the foils were electrochemically polished in a mixture of $HClO_4$ and C_2H_6O (1:4 volume ratio). As a final step of foil preparation, the Ni foils were annealed at 1000 °C for 8 h in a gas mixture of 90% Ar and 10% H_2 in order to decrease the internal stress and to further improve the crystalline quality. After these polishing and annealing procedures, the Ni foils were placed at the middle of the furnace tube between the small tubes containing the $NiCl_2$ powder. For the growth, the quartz tube was evacuated to a background vacuum of a few mbar, and the furnace was heated up to 600 °C at a rate of 50 °C/min. Then, a mixture gas of Ar and O_2 was introduced with a constant flow rate of 100 sccm, and the pressure inside the quartz tube was maintained at 800 mbar. Finally, the furnace was heated up further to the growth temperature and maintained for 15 min. After the furnace was cooled to room temperature, a layer of green products was grown on the surface of the Ni foils.

Characterization. A JEOL JSM-6700F field emission scanning electron microscope (SEM) and a JEOL 2100 high resolution transmission electron microscope (HRTEM) were used to study the morphology and structure of the samples. The composition was determined by an attached energy-dispersive X-ray spectrometer (EDS). The X-ray diffraction (XRD) analysis was carried out using a Bruker AXS D8 Advanced powder diffractometer with Cu Kα radiation. Focused ion beam (FIB) milling was performed using a XT Nova Nanolab 200. The electrical characterizations were carried out at room temperature on a probe station equipped with a Keithley 4200 semiconductor parameter analyzer.

Acknowledgment. This work is supported by the Singapore National Research Foundation (RCA-08/018) and the Institute of Materials Research and Engineering.

Supporting Information Available: The change of Ni foil crystal quality after annealing; SEM image of the NiO NW arrays milled by focused ion beam; the TEM images of the nanowire with [220] growth direction; the weight change and the XRD patterns of the Ni foil taken at various growth stages used for further growth mechanism discussion. This material is available free of charge *via* the Internet at http://pubs.acs.org.

REFERENCES AND NOTES

1. Xia, Y. N.; Yang, P. D.; Sun, Y. G.; Wu, Y. Y.; Mayers, B.; Gates, B.; Yin, Y. D.; Kim, F.; Yan, Y. Q. One-Dimensional Nanostructures: Synthesis, Characterization, and Applications. *Adv. Mater.* **2003**, *15*, 353–389.
2. Wagner, R. S.; Ellis, W. C. Vapor−Liquid−Solid Mechanism of Single Crystal Growth. *Appl. Phys. Lett.* **1964**, *4*, 89–90.

3. Morales, A. M.; Lieber, C. M. A Laser Ablation Method for the Synthesis of Crystalline Semiconductor Nanowires. *Science* **1998**, *279*, 208–211.
4. Bao, X. Y.; Soci, C.; Susac, D.; Bratvold, J.; Aplin, D. P. R.; Wei, W.; Chen, C. Y.; Dayeh, S. A.; Kavanagh, K. L.; Wang, D. L. Heteroepitaxial Growth of Vertical GaAs Nanowires on Si(111) Substrates by Metal−Organic Chemical Vapor Deposition. *Nano Lett.* **2008**, *8*, 3755–3760.
5. Duan, X. F.; Lieber, C. M. General Synthesis of Compound Semiconductor Nanowires. *Adv. Mater.* **2000**, *12*, 298–302.
6. Persson, A. I.; Larsson, M. W.; Stenstrom, S.; Ohlsson, B. J.; Samuelson, L.; Wallenberg, L. R. Solid-Phase Diffusion Mechanism for GaAs Nanowire Growth. *Nat. Mater.* **2004**, *3*, 677–681.
7. Pan, Z. W.; Dai, Z. R.; Wang, Z. L. Nanobelts of Semiconducting Oxides. *Science* **2001**, *291*, 1947–1949.
8. Bierman, M. J.; Lau, Y. K. A.; Kvit, A. V.; Schmitt, A. L.; Jin, S. Dislocation-Driven Nanowire Growth and Eshelby Twist. *Science* **2008**, *320*, 1060–1063.
9. Jiang, X. C.; Herricks, T.; Xia, Y. N. CuO Nanowires Can Be Synthesized by Heating Copper Substrates in Air. *Nano Lett.* **2002**, *2*, 1333–1338.
10. Hulteen, J. C.; Martin, C. R. A General Template-Based Method for the Preparation of Nanomaterials. *J. Mater. Chem.* **1997**, *7*, 1075–1087.
11. Mott, N. Metal-Insulator Transitions. *Phys. Today* **1978**, *31*, 42–47.
12. Adler, D.; Feinleib, J. Electrical and Optical Properties of Narrow-Band Materials. *Phys. Rev. B* **1970**, *2*, 3112–3134.
13. Li, Y.; Zhang, B. C.; Xie, X. W.; Liu, J. L.; Xu, Y. D.; Shen, W. J. Novel Ni Catalysts for Methane Decomposition to Hydrogen and Carbon Nanofibers. *J. Catal.* **2006**, *238*, 412–424.
14. Sreethawong, T.; Suzuki, Y.; Yoshikawa, S. Photocatalytic Evolution of Hydrogen over Mesoporous TiO_2 Supported NiO Photocatalyst Prepared by Single-Step Sol-Gel Process with Surfactant Template. *Int. J. Hydrogen Energy* **2005**, *30*, 1053–1062.
15. Hotovy, I.; Huran, J.; Spiess, L.; Hascik, S.; Rehacek, V. Preparation of Nickel Oxide Thin Films for Gas Sensors Applications. *Sens. Actuators B* **1999**, *57*, 147–152.
16. Poizot, P.; Laruelle, S.; Grugeon, S.; Dupont, L.; Tarascon, J. M. Nano-Sized Transition-Metaloxides as Negative-Electrode Materials for Lithium-Ion Batteries. *Nature* **2000**, *407*, 496–499.
17. Jiao, Z.; Wu, M. G.; Qin, Z.; Xu, H. The Electrochromic Characteristics of Sol-Gel-Prepared NiO Thin Film. *Nanotechnology* **2003**, *14*, 458–461.
18. Lewis, F. B.; Saunders, N. H. Thermal-Conductivity of NiO and CoO at Neel Temperature. *J. Phys. C* **1973**, *6*, 2525–2532.
19. Miller, E. L.; Rocheleau, R. E. Electrochemical Behavior of Reactively Sputtered Iron-Doped Nickel Oxide. *J. Electrochem. Soc.* **1997**, *144*, 3072–3077.
20. Kumagai, H.; Matsumoto, M.; Toyoda, K.; Obara, M. Preparation and Characteristics of Nickel Oxide Thin Film by Controlled Growth with Sequential Surface Chemical Reactions. *J. Mater. Sci. Lett.* **1996**, *15*, 1081–1083.
21. Chae, S. C.; Lee, J. S.; Kim, S.; Lee, S. B.; Chang, S. H.; Liu, C.; Kahng, B.; Shin, H.; Kim, D. W.; Jung, C. U.; *et al*. Random Circuit Breaker Network Model for Unipolar Resistance Switching. *Adv. Mater.* **2008**, *20*, 1154–1159.
22. Lee, M. J.; Seo, S.; Kim, D. C.; Ahn, S. E.; Seo, D. H.; Yoo, I. K.; Baek, I. G.; Kim, D. S.; Byun, I. S.; Kim, S. H.; *et al*. A Low-Temperature-Grown Oxide Diode as a New Switch Element for High-Density, Nonvolatile Memories. *Adv. Mater.* **2007**, *19*, 73–76.
23. Xu, C. K.; Hong, K. Q.; Liu, S.; Wang, G. H.; Zhao, X. N. A Novel Wet Chemical Route to NiO Nanowires. *J. Cryst. Growth* **2003**, *255*, 308–312.
24. Yang, Q.; Sha, J.; Ma, X. Y.; Yang, D. R. Synthesis of NiO Nanowires by a Sol-Gel Process. *Mater. Lett.* **2005**, *59*, 1967–1970.
25. Kim, S. I.; Lee, J. H.; Chang, Y. W.; Hwang, S. S.; Yoo, K. H. Reversible Resistive Switching Behaviors in NiO Nanowires. *Appl. Phys. Lett.* **2008**, *93*, 033503.
26. Lin, Y.; Xie, T.; Cheng, B. C.; Geng, B. Y.; Zhang, L. D. Ordered Nickel Oxide Nanowire Arrays and Their Optical Absorption Properties. *Chem. Phys. Lett.* **2003**, *380*, 521–525.
27. Zhan, Y. J.; Zheng, C. L.; Liu, Y. K.; Wang, G. H. Synthesis of NiO Nanowires by an Oxidation Route. *Mater. Lett.* **2003**, *57*, 3265–3268.
28. Xing, G. Z.; Yi, J. B.; Tao, J. G.; Liu, T.; Wong, L. M.; Zhang, Z.; Li, G. P.; Wang, S. J.; Ding, J.; Sum, T. C.; *et al*. Comparative Study of Room-Temperature Ferromagnetism in Cu-Doped ZnO Nanowires Enhanced by Structural Inhomogeneity. *Adv. Mater.* **2008**, *20*, 3521–3527.
29. Xing, G. Z.; Yi, J. B.; Wang, D. D.; Liao, L.; Yu, T.; Shen, Z. X.; Huan, C. H. A.; Sum, T. C.; Ding, J.; Wu, T. Strong Correlation between Ferromagnetism and Oxygen Deficiency in Cr-Doped In_2O_3 Nanostructures. *Phys. Rev. B* **2009**, *79*, 174406.
30. Chen, R.; Xing, G. Z.; Gao, J.; Zhang, Z.; Wu, T.; Sun, H. D. Characteristics of Ultraviolet Photoluminescence from High Quality Tin Oxide Nanowires. *Appl. Phys. Lett.* **2009**, *95*, 061908.
31. Lee, Y. Y.; McNallan, M. J. Ignition of Nickel in Environments Containing Oxygen and Chlorine. *Metall. Trans. A* **1987**, *18*, 1099–1107.
32. Chevalier, S.; Desserrey, F.; Larpin, J. Oxygen Transport During the High Temperature Oxidation of Pure Nickel. *Oxid. Met.* **2005**, *64*, 219–234.
33. Young, D. J. *High Temperature Oxidation and Corrosion of Metals*; Elsevier: Oxford, 2008; Vol. 1.
34. Jessensky, O.; Muller, F.; Gosele, U. Self-Organized Formation of Hexagonal Pore Arrays in Anodic Alumina. *Appl. Phys. Lett.* **1998**, *72*, 1173–1175.
35. Woodcock, T. G.; Abell, J. S.; Eickemeyer, J.; Holzapfel, B. Crystal Orientation Mapping of NiO Grown on Cube Textured Ni Tapes. *J. Microsc.-Oxford* **2004**, *216*, 123–130.
36. Mrowec, S. On Mechanism of High Temperature Oxidation of Metals and Alloys. *Corros. Sci.* **1967**, *7*, 563–578.
37. Kim, C. Joo.; Kang, K.; Woo, Y. S.; Ryu., K. G.; Moon, H.; Kim, J. M.; Zang, D. S.; Jo, M.-H. Spontaneous Chemical Vapor Growth of NiSi Nanowires and Their Metallic Properties. *Adv. Mater.* **2007**, *19*, 3637–3642.
38. Kang, K.; Kim, S. K.; Kim, C. J.; Jo, M.-H. The Role of NiO_x Overlayers on Spontaneous Growth of $NiSi_x$ Nanowires from Ni Seed Layers. *Nano Lett.* **2008**, *8*, 431–436.
39. Peng, K. Q.; Xu, Y.; Wu, Y.; Yan, Y. J.; Lee, S. T.; Zhu, J. Aligned Single-Crystalline Si Nanowire Arrays for Photovoltaic Applications. *Small* **2005**, *1*, 1062–1067.
40. Peng, K. Q.; Yan, Y. J.; Gao, S. P.; Zhu, J. Synthesis of Large-Area Silicon Nanowire Arrays *via* Self-Assembling Nanoelectrochemistry. *Adv. Mater.* **2002**, *14*, 1164–1167.
41. Stamplecoskie, K. G.; Ju, L.; Farvid, S. S.; Radovanovic, P. V. General Control of Transition-Metal-Doped GaN Nanowire Growth: Toward Understanding the Mechanism of Dopant Incorporation. *Nano Lett.* **2008**, *8*, 2674–2681.
42. Peraldi, R.; Monceau, D.; Pieraggi, B. Correlations between Growth Kinetics and Microstructure for Scales Formed by High-Temperature Oxidation of Pure Nickel. II. Growth Kinetics. *Oxid. Met.* **2002**, *58*, 275–295.
43. Ahn, S. E.; Lee, M. J.; Park, Y.; Kang, B. S.; Lee, C. B.; Kim, K. H.; Seo, S.; Suh, D. S.; Kim, D. C.; Hur, J.; *et al*. Write Current Reduction in Transition Metal Oxide Based Resistance-Change Memory. *Adv. Mater.* **2008**, *20*, 924–928.
44. Chang, S. H.; Lee, J. S.; Chae, S. C.; Lee, S. B.; Liu, C.; Kahng, B.; Kim, D. W.; Noh, T. W. Occurrence of Both Unipolar Memory and Threshold Resistance Switching in a NiO Film. *Phys. Rev. Lett.* **2009**, *102*, 026801.
45. Oka, K.; Yanagida, T.; Nagashima, K.; Tanaka, H.; Kawai, T. Nonvolatile Bipolar Resistive Memory Switching in Single Crystalline NiO Heterostructured Nanowires. *J. Am. Chem. Soc.* **2009**, *131*, 3434–3435.
46. JANAF Thermochemical Tables. J. Phys. Chem. Ref. Data **1975**, *4* (Suppl 1975), 79.